Journal of High Energy Physics, Gravitation and Cosmology, 2025, 11(3), 1107-1121
https://www.scirp.org/journal/jhepgc
ISSN Online: 2380-4335
ISSN Print: 2380-4327

Small Field Photon and Electron Beam Dosimetry Using Various Radiation Detectors

Md. Sahidul Islam[1*], Faruque Hossain Mozumder[2], Md. Matiur Rahman[3], Bilkish Akter[4], Shamsun Nahar Runa[1]

[1]Department of Physics, Govt. H. S. S. College, Magura, Bangladesh
[2]ICT Division, Jamuna Bank PLC., Dhaka, Bangladesh
[3]Department of Mathematics, Uttara University, Dhaka, Bangladesh
[4]Department of Economics, Govement Titumir College, Dhaka, Bangladesh
Email: *mannan.iu31@gmail.com

How to cite this paper: Islam, M.S., Mozumder, F.H., Rahman, M.M., Akter, B. and Runa, S.N. (2025) Small Field Photon and Electron Beam Dosimetry Using Various Radiation Detectors. *Journal of High Energy Physics, Gravitation and Cosmology*, **11**, 1107-1121.
https://doi.org/10.4236/jhepgc.2025.113071

Received: December 4, 2024
Accepted: July 25, 2025
Published: July 28, 2025

Abstract

The aim of this article is to study: 1) the dosimetric properties of various ionization chamber such as semi-flex and farmer chamber in comparison with diamond, pinpoint and diode detector with the moluminescence dosimetry for total scatter analysis and dose profile, and 2) flattening filter free (FFF) beams (output measurements, profile analysis, surface dose and consistency) generated by medical linear accelerator and its variation with respect to flattened beams (FB). With the appearance of new techniques such as intensity-modulated radiation therapy (IMRT), volumetric radiation therapy (SBRT), stereotactic radios surgery (SRS), applying relativity small fields that are either dynamic or static is needed. For this purpose, there have been many developments in treatment machines.

Keywords

Small Field Dosimetry, Diode Detector, Beam Data Commissioning, Cyber Knife

1. Introduction

The dosimetry of small field sizes is considerably unlike from that for standard radiotherapy field sizes. In low density medium similar to the lung, small fields have important perturbations that are energy and density dependent. According to the abovementioned challenges, selecting a detector with good performance in small fields is difficult. The necessary properties of a desired detector are high spatial resolution, high signal, low energy dependence, water equivalence, high

stability and easy to use clinically. Certainly, there is no standard dosimeter for a small field because no detector has all the aforementioned properties. Radiotherapy plays a leading role for the treatment of cancer patients in all over the world. External beam radiotherapy includes high energy photon and electron beam linear accelerator, tele-cobalt therapy, cyclotron-based proton beam therapy, reactor-based boron neutron capture therapy, low energy X-ray therapy, etc. The outcome of the radiotherapy is highly dependent on how pre visional dose deliver to the tumor which should not exceed 5% of the prescribed dose including all types uncertainties involved in the treatment procedure such as dosimetry, treatment planning and dose stability of the treatment unit. This implies that dose measurement should be accurate which lies within ±3.5% as per ICRU recommendation. In conventional radiotherapy with linear accelerator, radiation fields are characterized between 4 cm × 4 cm to 25 cm × 25 cm. The field size below 4 cm × 4 cm is considered as small field. The dosimetry of small-field is a challenging issue. The increased use of small fields in modern radiotherapy has created the demand for more standardization of dosimetry procedure and better understanding of these in non-reference small field conditions. For absorbed dose to water measurement of photon and electron beam above 4×4 cm^2 field sizes are already established and several protocols for dosimetry are already established by various international organizations such as IAEA (TRS-277, TRS-381, TRS-398), AAPM (TG-21, TG 51), DIN-6800-2. The deviation of dose measurements between the protocols lies within ±1.2%. To minimize the uncertainties still many laboratories has emphasized their research regarding the improvement of precision of dosimetry. What value of precision is required in radiotherapy!! Recently, IAEA has declared to revise their latest dosimetry protocol TRS-398. In photon and electron beam dosimetry, ideally a detector (volume: 0.125 cc to 0.6 cc) with high sensitivity, good spatial resolution, low energy dependence, good stability and tissue equivalence should be utilized and reference condition is also established. The absorbed dose to water measurement of aperture less than 4×4 cm^2 is a critical issue. Small cancerous lesions are typically treated with photon and electrons. Depending upon the size, shape and location of the lesion, the field aperture, commonly referred to as cutout, is custom-made using Cerrobend. Accurate dosimetry for such small fields is challenging due to the loss of lateral electronic equilibrium within the field. This can result in a shift of d_{max} towards the surface and other modifications of the depth dose curve, as well as a change in the beam profile characteristics at depth. Small (narrow or sub-centimeter) beam apertures are used for delivery of prescribed dose to patients by advanced photon beam radiotherapy techniques (intensity modulated radiotherapy, IMRT; image-guided radiotherapy, IGRT; stereotactic radio surgery/radiotherapy, SRS/SRT). Both standard and specialized (e.g. Cyber Knife and Tom therapy) medical electron linear accelerators with high resolution MLCs as well as specialized tele isotope machines (e.g. Gamma Knife) deliver treatments by using small photon fields ([1] [2]). The use of small photon fields is almost a pre-requisite for high precision

localized dose delivery to delineated target volume, sparing of organs at risk, and escalating the dose to the tumor for improved control of the disease (e.g. prostate). Thus, small-beam apertures are important for fulfilling the clinical goal of radiotherapy. However, such fields have inherent characteristics of charge particle disequilibrium and high-dose gradient, making dosimetry measurements challenging. A small photon field is generally defined as the one having dimensions smaller than the lateral range of the charged particles that contribute to the dose deposited at a point along the central axis of the beam. The main limitations of most dosimeters are insufficient spatial resolution, water nonequivalence, and energy dependence. In megavoltage (MV) photon beams from linear accelerators, small field conditions occur as a result of two scenarios. Firstly, as the collimator opening is made smaller the entire photon source is no longer visible from the measurement point and, secondly, the size of the radiation field becomes small in comparison to the maximum lateral range of secondary electrons. As a consequence, in a small field, a reduction in beam output is observed on the beam central axis, as well as a widening of the penumbra in the transverse direction as a result of overlapping penumbrae [3]. In recent years, with the growth in prescribed use of high doses per fraction in radio surgery and dose escalation cancer treatments, the dosimetry of high dose-rate FFF beams from modern study [4]. Hence, the dosimetry of small photon field presents many challenges, which are related to source occlusion, lateral electronic disequilibrium, and the choice of the detector. Radiation detectors such as diamond, pencil, diode detectors and thermos-luminescence dosimeter could be a leading device the leading devices to meet the current desirable characteristics.

The micro-Diamond has shown excellent characteristics, such as the small spatial resolution and stable response against the beam energy, dose rate and temperature ([5] [6]), although the cost is higher than for diodes ([7] [8]).

2. Design and Methods

The research program will thus include the following major phases of investigation:

- Selection of ionization chamber and its characteristics (semi-flex chamber, diode, pinpoint, and diamond chambers)
- Selection of phantom such as blue phantom or Alderson Rando Phantom or slab phantom for absorbed dose determinations
- Determination of absorbed dose to water for various field sizes (0.1 cm × 0.1 cm to 25 cm × 25 cm) using TRS-398
- Calculation of the total scattering factors for various field sizes
- Effect FB and FFF in treatment planning system
- Calibration of TL dosimeter
- Measurement of irradiated TLD by Harshaw TLD reader
- Analysis of experimental data for various measurement
- Theoretical analysis with Geant4/Fluke/MCNP code

The outline of the research program is more or less provided in the above. The final details or essential modifications etc. could be worked out as per advice made by supervisors and according to the facilities available (see Figure 1).

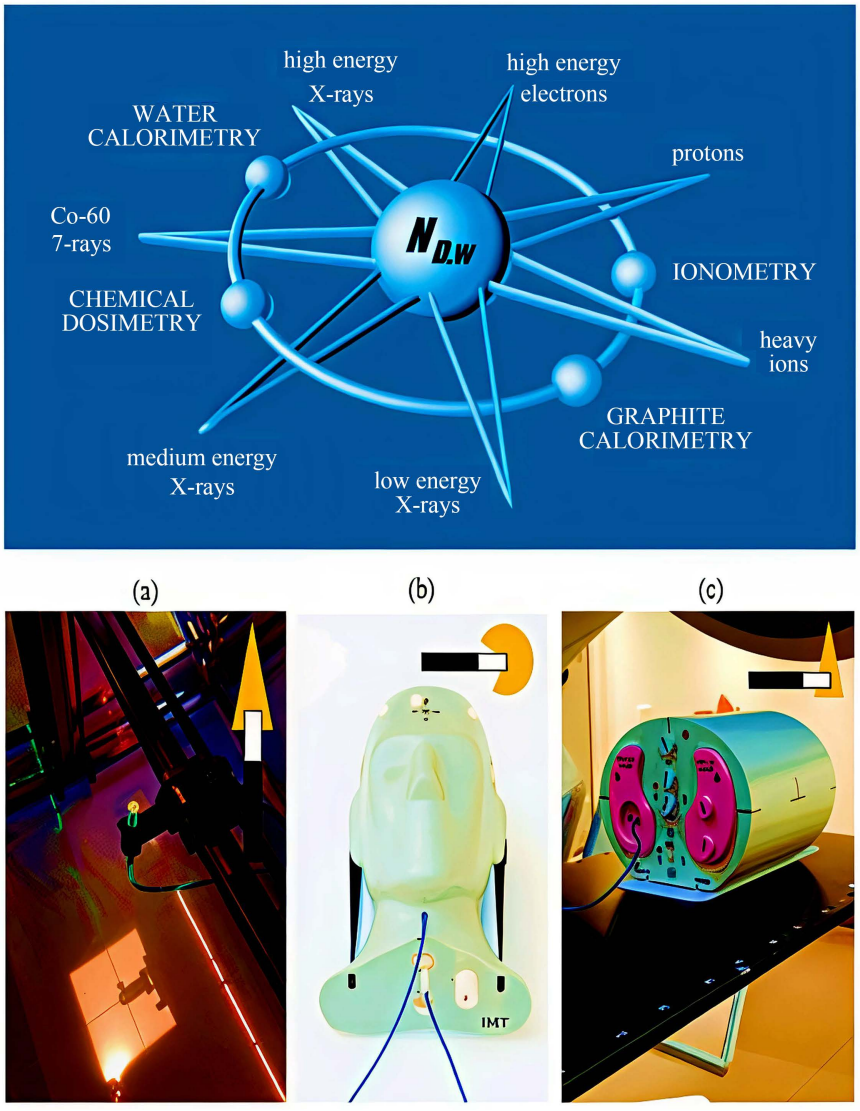

Figure 1. Diagram of medical radiation dosimetry and calibration equipment.

3. Purpose of the Design

This study clarified coplanar and non-coplanar beams using different types of detectors with the effect of angular dependence on small-field dosimetry. (Kohei kawata, Tomohiro ono, Hideaki hirashima {..}Manabu Nakata) ([9] [10]).

4. Types of Radiation and Range of Beam Qualities

This code of practice provides a methodology for the determination of absorbed dose to water in the low, medium and high energy photon beams, electron beams, proton beams and heavy ion beams used for external radiation therapy. Actually,

the range of radiation qualities covered in this report are given below (for a description of the beam quality index see the corresponding sections):

1) Low energy X-rays with generating potentials up to 100 kV ana HVL of 3 mm A1 (the lower limit is determined by the availability of standards); 4. The boundary between the two ranges for KV X-rays is not strict and has an overlap between 80 kV, 2 mm A1. In terms of overlap region, the various for absorbed dose determination given in site 8 or 9 are equally satisfactory, and whichever is more convenient should be used.

2) Medium energy X-rays with generating potentials above 80 kV and HVL of 2 mm A1.

3) ^{60}Co gamma radiation.

4) High energy photons generated by electrons with energies in the interval 1 - 50 Mev, with TPR20, 10 values between 0.50 and 0.84.

5) Electrons in the energy interval 3 - 50 Mev, with a half-value depth, R50, between 1 and 20 g/cm^2.

6) Protons in the energy interval 50 - 250 Mev, with a practical range, Rp, between 0.25 and 25 g/cm^2.

7) Heavy ions with Z between 2 (He) and 18 (Ar) having a practical range in water, Rp, of 2 to 30 g/cm^2 (for carbon ions this corresponds to an energy range of 100 Mev/u to 450 Mev/u, when u is the atomic mass unit.

5. Quantities and Symbols

Almost of the symbols utilized in this code of practice are identical to those used in major advance radiotherapy over the last few years has been the climb up use of proton and heavy ion irradiation convenient for radiation therapy. Practical dosimetry in this fields is also based on the use of ionization chambers that may be provided with calibrations each according to Air kerma and in terms of absorbed dose to water, therefore the dosimetry methods developed for high energy photon and electrons can also be applicable to heavy ions and protons. On the other extreme of the range available teletherapy beams lie KV X-ray beams, and for these the utilize of standards of absorbed dose to water was introduced in IAEA technical reports series no 277 (TRS-277), and only a few are new in the context of standards of absorbed dose to water. For completeness, a summary is provided here for all quantities of relevance to the different criteria used in this code of practice. There are a lot of symbols utilizes these methods. For instance,

C_{pl}: Material dependent scaling factor to convert ranges and depths measured in plastic phantoms into the equivalent values in water. Basically, this applies to electron, proton and heavy ion beams.

C_{sda}: Continious slowing down approximation.

Eo, Ez: An electron beam of energy at the pantom surface and at depth z respectively. Unit: *Mev*.

H_{pl}: Difference between electron fluence in plastic and water equivalent depth.

H_{VL}: Half-value layer, used as abeam quality index for low and medium energy X-ray beams.

K_{elec}: Calibration factor of an electrometer.

K_{pol}: Factor to correct the response of an ionization chamber for the effect of a change polarity of the polarizing voltage applied to the chamber.

K_s: Factor to correct the response of an ionization chamber for the lack of complete charge collection (due to ion recombination).

M_Q: *Reading* of dosimeter at quality Corrected for influence quantities other than beam quality. Unit: C or rdg.

$N_{k,Qo}$: Calibration factor in terms of air kerma for a dosimeter at a reference beam quality Qo. Unit: Gy/C or Gy/rdg.

P_{cav}: Factor that corrects the response of an ionization chamber for effects related to air cavity, predominantly the in -scattering of electrons that makes the electron fluence inside a cavity different from that in the medium in the absence of the cavity.

P_{DD}: percentage Depth Dose.

P_{wall}: Factor that corrects the response of an ionization chamber for the non-medium equivalence of the chamber wall and any waterproofing material.

Q: General symbol indicates the quality of a radiation beam. A subscript "O", *i.e.* Qo, indicates the reference quality used for the calibration of an ionization chamber or a dosimeter.

R_{dg}: Value, in arbitrary units, used for the reading of a dosimeter.

R_{50}: Half-value depth in water (in g/cm^2), used as the beam quality index for electron beams.

R_p: Practical range (in g/cm^2) for proton, electron and heavy ion beams.

R_{res}: Residual range (in g/cm^2) for proton beams.

R_{cyl}: Cavity radius of a cylindrical ionization chamber.

SAD: Source axis distance.

SCD: Source chamber distance.

SOBP: Spread out brag peak.

SSD: Source-surface distance.

TMR: Tissue maximum ratio.

$TPR_{20,10}$: Tissue phantom ratio in water at depths of 20 and 10 g/cm^2, for a field size of (10 × 10) cm and SCD of 100 cm, utilized as the beam quality index for high energy photon radiation.

u_c: Combined standard uncertainty of a quantity.

W_{air}: The mean energy expended in air per ion pair formed.

Z_{max}: Depth of maximum dose (in g/cm^2).

Z_{ref}: Reference depth (in g/cm^2) for pantom measurements. When specified at Zref, the absorbed dose to water refers to Dw, Q at the inter section of the beam central axix with plane defined by Zref.

And also has **Dw, Q, Ki, Kh, KQ, Q, KTP, Mem**, **ND, air, ND, W, Qo, Pcel, Pdis, Peff, PQ**.

6. Temperature Dependence

By changing water temperature with a flattening filter (WFF), which temperature

was evaluated by irradiating a 6 MV Photon beam. Actually, the micro silicon and diode E detectors were located at a 10 cm below from the entrance window of the water phantom model GRI-7670A (Toyo-Medic, Tokyo, Japan) [10] that was scheme to measure lateral beams. According to the field size, gantry angle and source to surface difference (SSD) were 100 × 100 mm^2, 270 degree and 90 cm respectively. At first, measurements were repeated by replacing little bit cold water with hot water, cold water was poured into the phantom. In terms of the course of the experiments, from 11.5 to 31.3-degree Celsius water temperature was boosted. Because diode E was much lower than the response of the microsilicon, the detector readings were normalized at 21.5 degree Celsius and relative methods were compared.

1) Saini AS, Zhu TC (temperature dependence of commercially available diode detectors. Med Phy 2002; 29: 622-630

2) Scherf C, Peter C, Moog J *et al.*, Silicon diodes as an alternative to diamond detectors for depth dose curves and profile measurements of photon and electron radiation. Strahlenther Onkol 2009; 185: 530-536

7. Expected Results and Impact

Figure 2 illustrates the temperature dependence of the Diode E and micro-Silicon detectors. The Diode E exhibited a positive correlation of the response to temperature, and the difference between 11.5˚C and 31.3˚C was 5.06%. When calculating the linear regression, the variation of the readings was 0.26%/˚C. In contrast, the micro-Silicon diode yielded very small variations within the range from −0.33% to 0.06%. Figure 3(a) depicts the dose-response linearity for various detectors. Values were normalized at 100 MU. All detectors showed good linearity (R_2 = 1.000 for all detectors). Figure 3(b) shows the readings of each detector divided by the irradiated dose. Most detectors, including the Farmer-type ionization chamber, showed large variations for irradiation < 10 cGy, likely due to the instability of the beam output. For irradiation ≥ 10 cGy, all detectors showed excellent linearity within 0.5%.

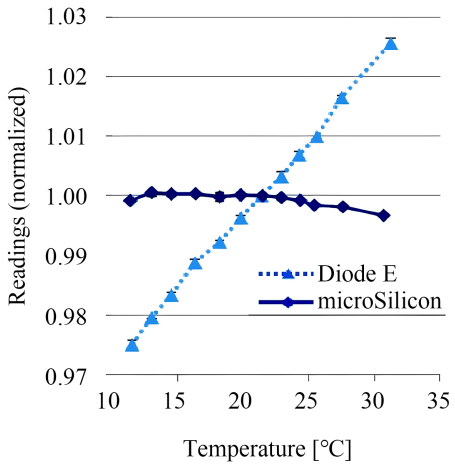

Figure 2. Temperature dependence of diode e and microsilicon readings.

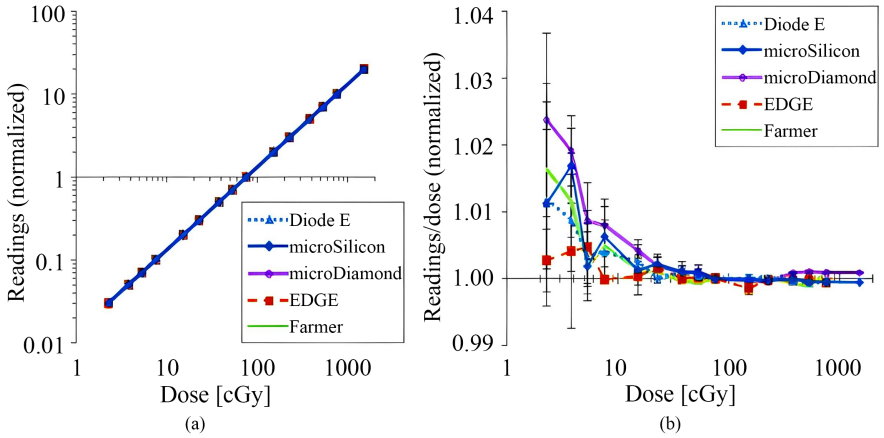

Figure 3. (a) Linearity of the detectors for 6 MV photon beams. Both horizontal and vertical axes are log scale. The values were normalized at 76.1 cGy (100 MU). (b) The detector readings divided by the irradiated dose, normalized at 100 MU. The points and bars represent the mean and standard deviation of measurements, respectively. Only the horizontal axis is log scale.

In **Figure 4**, the detector readings divided by irradiated dose (nC/cGy) normalized at 400 MU/min dose rate were plotted against the dose rate. For all measurements, the CV of measurements was within 0.2%. For 6 MV and 10 MV photon beams, the values of the WFF and FFF beams were plotted in the same figure, which clearly shows the dose rate.

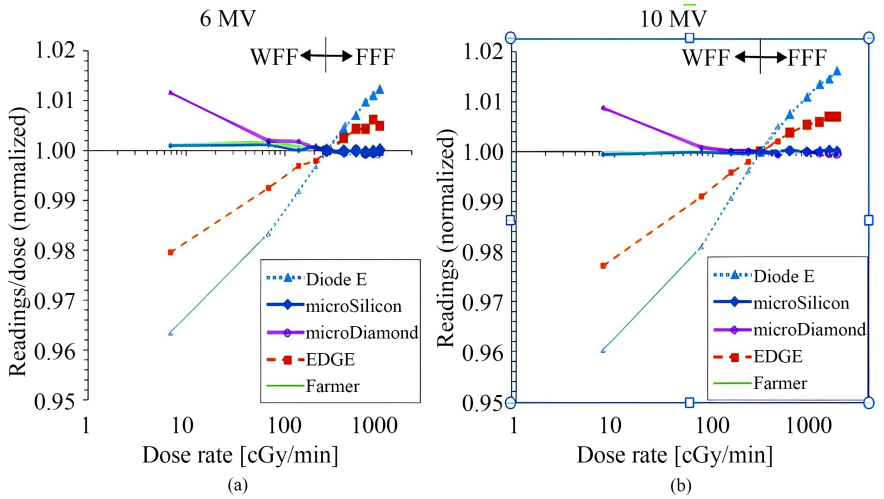

Figure 4. The dose rate dependence of the detectors for (a) 6 MV and (b) 10 MV with flattening filter (WFF) and flattening filter free (FFF) beams. The detector readings divided by the irradiated dose were normalized at 400 MU/min dose rate. The small and large points represent the WFF and FFF beams, respectively.

Figure 3 shows temperature dependence of the Diode E and micro-Silicon detectors. The electrometer readings of the electro-meter were normalized at 21.5˚C. dependence of the Diode E and EDGE detectors, whereas the microSil-icon showed a stable response. Because the horizontal axis is log scale, the linear plots

represent the logarithmic correlation between the dose rate and the detector readings. The Farmer-type ionization cham be with corrections also yielded a stable response. The microdiamond demonstrated an increased response only at a 10-MU/min dose rate.

Figure 5 shows the energy dependence of each detector evaluated for a 400 MU/min dose rate. The variations of the ionization chamber, micro-Diamond and EDGE detectors were within 1%. On the other hand, the Diode E and micro-Silicon detectors exhibited negative correlations between the response and TPR20, 10, and the micro-Silicon showed larger energy dependence.

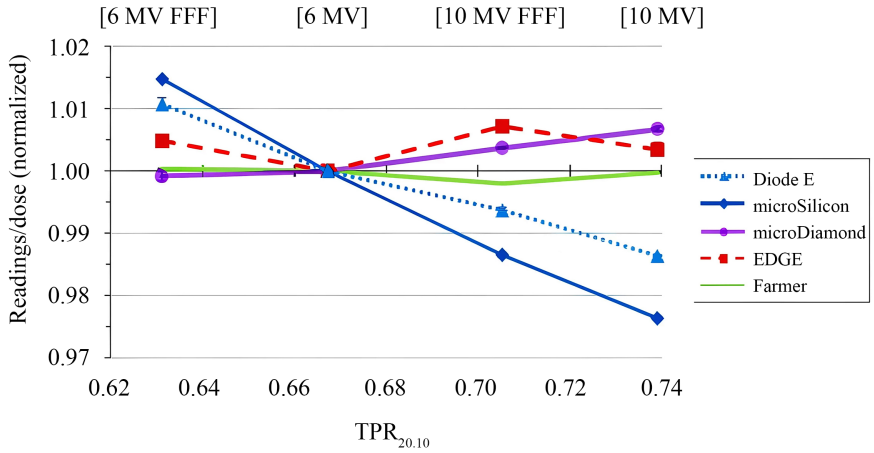

Figure 5. The detector readings divided by the irradiated dose normalized by the value of the 6 MV WFF beam are plotted against theTPR20, 10 (tissue-phantom ratio) of each beam energy.

Figure 6 and Figure 7 show the OF det and Ωfclin, fmsr, Qclin, Qmsr values of the True-Beam STx, respectively. In Figure 5, the OF det are shown in insets, and the relative differences from the Ωfclin, fmsr, Qclin, Qmsr values of the micro-Diamond were plotted. For all measurements the CV was within 0.1%. For ≤20 × 20 mm^2 field sizes, the micro-Silicon demonstrated the smallest OFdet values of all detectors, whereas the EDGE detector showed the largest values. For the 5 × 5 mm^2 field size, the mean difference of the four beam energies were 7.4%, 1.6%, 3.8% and 8.4% for the Diode E, micro-Silicon, micro-Diamond and EDGE detectors, respectively.

Figure 7 shows the Ωfclin, fmsr, Qclin, Qmsr values of the Diode E, micro-Diamond and EDGE detectors, as well as the OF det values of the micro-Silicon detector in insets, and the relative difference of each value from the Ωfclin, fmsr, Qclin, Qmsr of the microdiamond is also shown. For the 5 × 5 mm^2 field size, the mean difference of the four beam energies were 1.4% and 0.8% for the Diode E and EDGE detectors, respectively. Although the values of the micro-Silicon detector were not corrected by the output correction factors, values were not significantly different from the Ωfclin, fmsr, Qclin, Qmsr of other detectors. The mean difference between the OF det of the micro-Silicon and the Ωfclin, fmsr, Qclin,

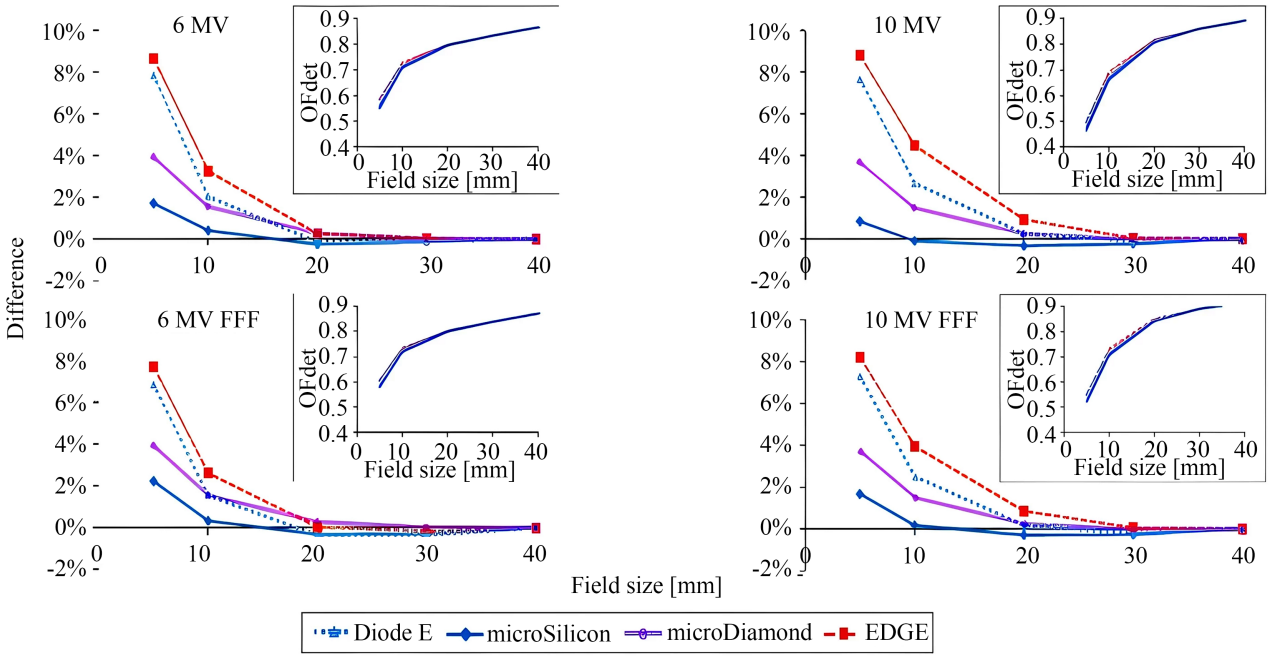

Figure 6. The detector output factors (OFdet) of TrueBeam STx plotted against the square field sizes (insets) and the relative difference of each value from the field output factor (Ωfclin, fmsr, Qclin, Qmsr) of the micro-Diamond detector. data from the micro-Diamond data. The PDD demonstrates small variations within 1% in the dose fall-off region. The micro-Silicon detector yielded the smallest difference from the micro-Diamond profile data. The micro-Silicon and micro-Diamond detectors showed similar penumbra widths, whereas the EDGE and Diode E detectors showed steeper penumbra profiles. **Figure 6** shows the PDD and beam profiles of the Cyber Knife beams. The variations of the PDD were within 1.3% in the dose fall-off region. The micro-Silicon showed similar beam profiles to those of micro-Diamond, whereas the Diode E and Diode SRS showed slightly steeper penumbra shape.

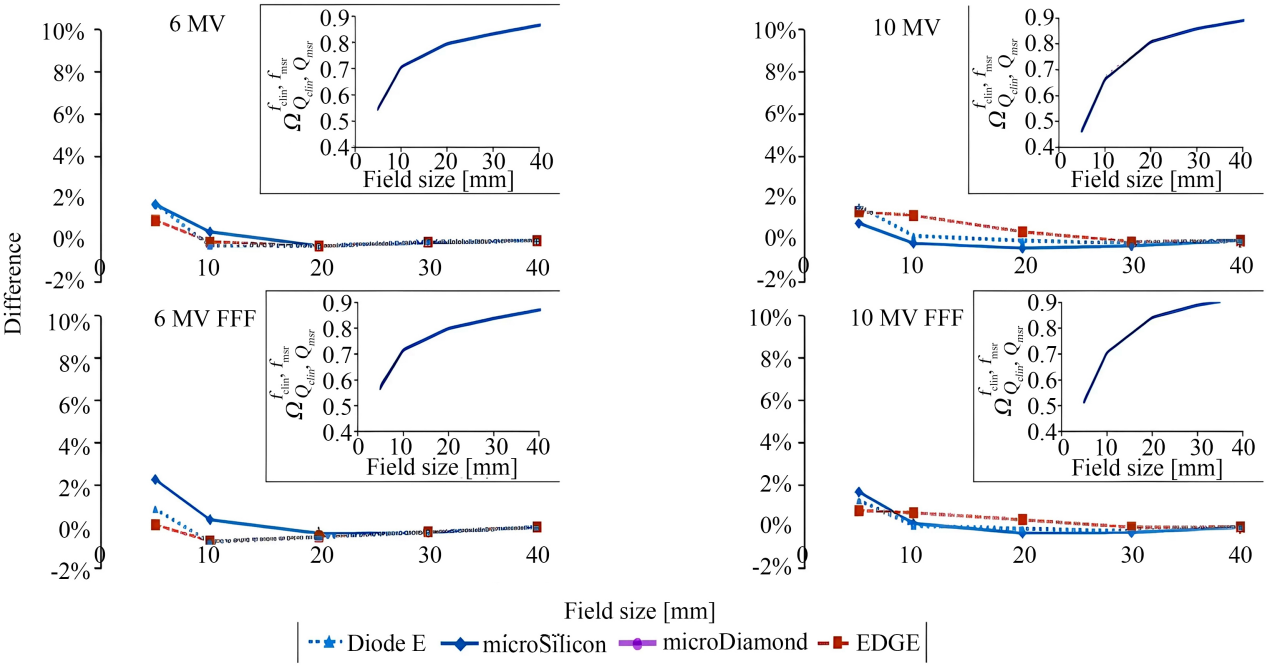

Figure 7. The field output factor (Ωfclin, fmsr, Qclin, Qmsr) of TrueBeam STx plotted against the square field sizes (insets) and the relative difference of each value from the Ωfclin, fmsr, Qclin, Qmsr of the micro-Diamond detector. OFdet values are plotted only for the micros icon detector.

Qmsr of the micro-Diamond was 1.6%. Similar results were obtained from the OFdet and Ωfclin, fmsr, Qclin, Qmsr of the Cyber Knife data (Figure 8). The OF det of the Diode E and micro-Silicon at 100 × 100 mm² field size was ~1.01, indicating the overresponse probably because of the scattered photons with low energy. If the values were normalized at 100 × 100 mm² field size, the values of these detectors at small fields would be underestimated.

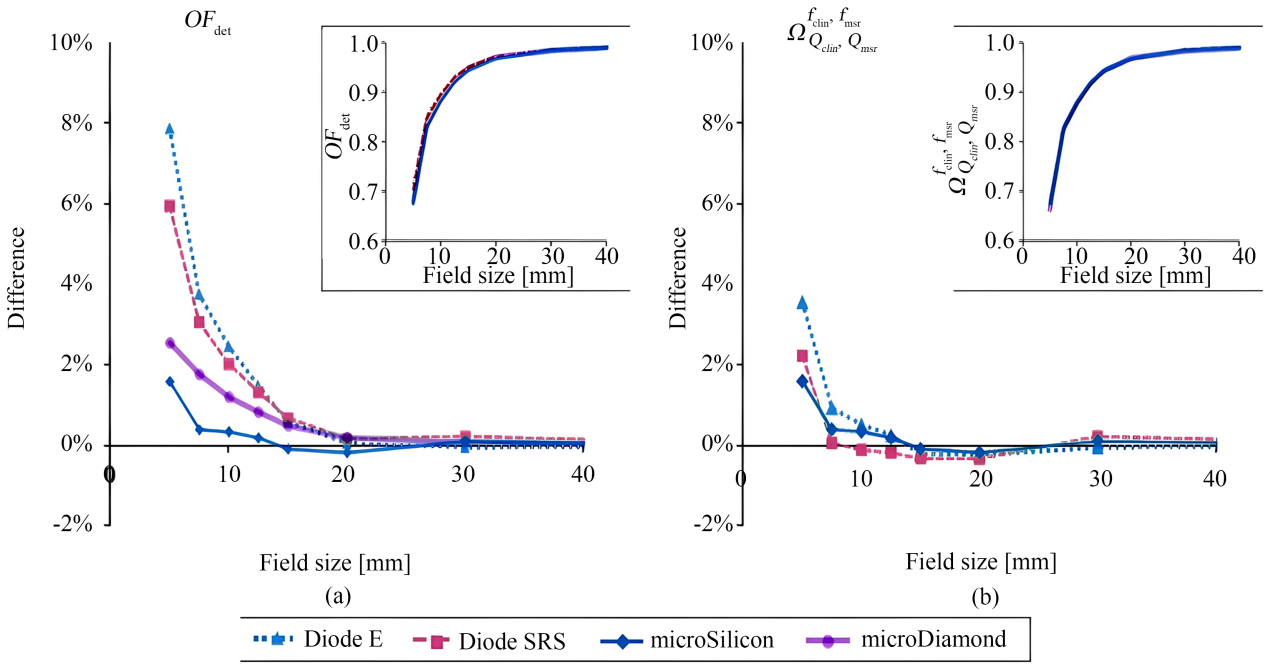

Figure 8. (a) The detector output factors (OFdet) and (b) field output factor (Ωfclin, fmsr, Qclin, Qmsr) of Cyber Knife plotted against the nominal cone diameter (Insets) and the relative difference of each value from the Ωfclin, fmsr, Qclin, Qmsr of the micro-Diamond detector. OF det values are plotted only for the micro-Silicon detector.

Advance in radiotherapy techniques are resulting in more frequent use of smaller field sizes, necessitating dosimeters of high spatial resolution and tissue equivalence. The outline of this research program is to measure total scattering factors and impact of chambers for small field dosimetry hence the result from this thesis program could be useful in treatment planning for small lesion. The analyzed data for FB and FFF would be useful for future reference and commissioning of linear accelerator for small field considerations.

8. Result and Discussion

The properties of the micro-Silicon diode for small-field photon beam dosimetry were examined in this work. The features of the micro-Silicon detector were recently disclosed by Schönfeld *et al.* [11]. The temperature dependence, energy dependence, and assessment of the Cyber Knife's smaller fields collimated by cones are among the extra data we present in this study. In contrast to the Diode E detector, which had a temperature-dependent response variation of 0.26%/˚C, we showed that the micro-Silicon detector produces stable responses across a broad

range of water temperatures. Akino *et al.* previously found a slight change in response for the micro-Diamond detector in the temperature range of 4˚C - 41˚C, within 0.7%. According to reports, the plastic scintillator exhibits a temperature-dependent reaction [12]. A temperature-independent detector will yield more stable data, even though the effect on the data recorded in a water phantom might not be significant. Additionally, the micro-Silicon showed extremely tiny fluctuation against the dosage rate, however there were variations in the response that were energy dependent. The Diode E, EDGE, and micro-Diamond, on the other hand, showed change with dose rate. While the EDGE and microdiamond displayed minor fluctuations of less than 1%, Diode E also displayed an energy dependence resembling that of micro-Silicon. At a very low dose rate, the micro-Diamond demonstrated a modest increase in responsiveness. Similar results were previously reported for electron beams by Björk *et al.* [13]. Numerous investigations have documented the diode and diamond detectors, showed a response that was dependent on the dose per pulse (DPP) [14]. According to Schönfeld *et al.*, the Diode E demonstrated a DPP-dependent increase in response of up to 3%, while the micro-Silicon and micro-Diamond detectors had minimal DPP dependence [15]. Information from the seller indicates that the dosage rate settings have no effect on the MU-per-pulse of the photon beams produced by the TrueBeam linear accelerator (personal communication). Consequently, the DPP dependence of the detectors had no effect on the dose rate dependence seen in this investigation. DPP may have an impact on the energy dependence depicted in **Figure 4**. When the measurements were set, the DPP values for 6 MV FFF, 6 MV WFF, 10 MV FFF, and 10 MV WFF were 0.546, 0.214, 1.034, and 0.233 mGy/pulse. Although the micro-Silicon detector showed characteristics suitable for small field dosimetry, the detector exhibited over-response for large field measurements (data not shown). When the OFdet of the 6 MV WFF beam was re-normalized at the 40×40 mm^2 field size to the value measured with a CC13 ionization chamber, the relative differences of the OFdet of the 100×100 mm^2 field size relative to the value of CC13 were 1.2%, 0.9%, 0.3% and −0.3% for the Diode E, micro-Silicon, EDGE and micro-Diamond, respectively. For the 220×220 mm^2 field size, the relative differences were 4.6%, 4.0%, 2.6% and −0.2%, respectively. For middle–large field sizes, ionization chambers provide more reliable. The micro-Diamond has shown excellent characteristics, such as the small spatial resolution and stable response against the beam energy, dose rate and temperature, although the cost is higher than for diodes.

9. Conclusion

We examined the properties of the micro-Silicon diode detector for small-field photon beam dosimetry. Compared to the Diode E, the micro-Silicon detector produced less variance with water temperature and dose rate. Additionally, the scanning data and scatter factor showed that the micro-Silicon detector offers suitable data for modest field experiments. The micro-Silicon offers suitable data for small field dosimetry when used carefully.

Acknowledgements

I would like to thank my respectable teacher Prof. Dr. Moqbul Hossain for guidance throughout the research process. Authors have made equal contributions for paper.

Conflicts of Interest

The authors declare that they have no competing interests.

References

[1] Scott, A.J.D., Kumar, S., Nahum, A.E. and Fenwick, J.D. (2012) Characterizing the Influence of Detector Density on Dosimeter Response in Non-Equilibrium Small Photon Fields. *Physics in Medicine and Biology*, **57**, 4461-4476. https://doi.org/10.1088/0031-9155/57/14/4461

[2] Fenwick, J.D., Kumar, S., Scott, A.J.D. and Nahum, A.E. (2013) Using Cavity Theory to Describe the Dependence on Detector Density of Dosimeter Response in Non-Equilibrium Small Fields. *Physics in Medicine and Biology*, **58**, 2901-2923. https://doi.org/10.1088/0031-9155/58/9/2901

[3] Underwood, T.S.A., Winter, H.C., Hill, M.A. and Fenwick, J.D. (2013) Detector Density and Small Field Dosimetry: Integral versus Point Dose Measurement Schemes. *Medical Physics*, **40**, Article ID: 082102. https://doi.org/10.1118/1.4812687

[4] Cranmer-Sargison, G., Weston, S., Evans, J.A., Sidhu, N.P. and Thwaites, D.I. (2012) Monte Carlo Modelling of Diode Detectors for Small Field MV Photon Dosimetry: Detector Model Simplification and the Sensitivity of Correction Factors to Source Parameterization. *Physics in Medicine and Biology*, **57**, 5141-5153. https://doi.org/10.1088/0031-9155/57/16/5141

[5] Charles, P.H., Crowe, S.B., Kairn, T., Kenny, J., Lehmann, J., Lye, J., *et al.* (2012) The Effect of Very Small Air Gaps on Small Field Dosimetry. *Physics in Medicine and Biology*, **57**, 6947-6960. https://doi.org/10.1088/0031-9155/57/21/6947

[6] Charles, P.H., Crowe, S.B., Kairn, T., Knight, R.T., Hill, B., Kenny, J., *et al.* (2013) Monte Carlo-Based Diode Design for Correction-Less Small Field Dosimetry. *Physics in Medicine and Biology*, **58**, 4501-4512. https://doi.org/10.1088/0031-9155/58/13/4501

[7] Scherf, C., Peter, C., Moog, J., Licher, J., Kara, E., Zink, K., *et al.* (2009) Silicon Diodes as an Alternative to Diamond Detectors for Depth Dose Curves and Profile Measurements of Photon and Electron Radiation. *Strahlentherapie und Onkologie*, **185**, 530-536. https://doi.org/10.1007/s00066-009-2004-x

[8] Reggiori, G., Mancosu, P., Suchowerska, N., Lobefalo, F., Stravato, A., Tomatis, S., *et al.* (2016) Characterization of a New Unshielded Diode for Small Field Dosimetry under Flattening Filter Free Beams. *Physica Medica*, **32**, 408-413. https://doi.org/10.1016/j.ejmp.2016.02.004

[9] Brualla-González, L., Gómez, F., Pombar, M. and Pardo-Montero, J. (2015) Dose Rate Dependence of the PTW 60019 Microdiamond Detector in High Dose-Per-Pulse Pulsed Beams. *Physics in Medicine and Biology*, **61**, N11-N19. https://doi.org/10.1088/0031-9155/61/1/n11

[10] Reggiori, G., Stravato, A., Pimpinella, M., Lobefalo, F., De Coste, V., Fogliata, A., *et al.* (2017) Use of PTW-Microdiamond for Relative Dosimetry of Unflattened Photon Beams. *Physica Medica*, **38**, 45-53. https://doi.org/10.1016/j.ejmp.2017.05.046

[11] Akino, Y., Mizuno, H., Tanaka, Y., Isono, M., Masai, N. and Yamamoto, T. (2018) Inter-institutional Variability of Small-Field-Dosimetry Beams among HD120™ Multileaf Collimators: A Multi-Institutional Analysis. *Physics in Medicine & Biology*, **63**, Article ID: 205018. https://doi.org/10.1088/1361-6560/aae450

[12] Beddar, A.S., Mason, D.J. and O'Brien, P.F. (1994) Absorbed Dose Perturbation Caused by Diodes for Small Field Photon Dosimetry. *Medical Physics*, **21**, 1075-1079. https://doi.org/10.1118/1.597350

[13] Lárraga-Gutiérrez, J.M., Ballesteros-Zebadúa, P., Rodríguez-Ponce, M., García-Garduño, O.A. and de la Cruz, O.O.G. (2015) Properties of a Commercial PTW-60019 Synthetic Diamond Detector for the Dosimetry of Small Radiotherapy Beams. *Physics in Medicine and Biology*, **60**, 905-924. https://doi.org/10.1088/0031-9155/60/2/905

[14] Veselsky, T., Novotny, J., Pastykova, V. and Koniarova, I. (2017) Determination of Small Field Synthetic Single-Crystal Diamond Detector Correction Factors for Cyberknife, Leksell Gamma Knife Perfexion and Linear Accelerator. *Physica Medica*, **44**, 66-71. https://doi.org/10.1016/j.ejmp.2017.11.010

[15] De Coste, V., Francescon, P., Marinelli, M., Masi, L., Paganini, L., Pimpinella, M., *et al.* (2017) Is the PTW 60019 Microdiamond a Suitable Candidate for Small Field Reference Dosimetry? *Physics in Medicine & Biology*, **62**, 7036-7055. https://doi.org/10.1088/1361-6560/aa7e59

Abbreviations of Organizations

The following abbreviations are used in this report to refer to different organizations involved in radiation dosimetry:

ARPANSA	Australian Radiation Protection and Nuclear Safety Agency, Australia.
BEV	Bundesamt für Eich- und Vermessungswesen, Austria
BIPM	Bureau International des Poids et Mesures
CCEMRI(I)	Comité Consultatif pour les Etalons de Mesure Mesure des RayonnementsIonisants (Section I) (Consultative Committee for Standards of Ionizing Radiation). Since September 1997, the CCEMRI and its sections have been renamed CCRI
CCRI(I)	Comité Consultatif des Rayonnements Ionisants (Section I) (Consultative Committee for Ionizing Radiation)
CIPM	Comité International des Poids et Mesures
ENEA	Ente per le Nuove Tecnologie, l'Energia e l'Ambiente, Institution.
INMRI	Nazionale di Metrologia delle Radiazioni Ionizzanti, Italy
ICRU	International Commission on Radiation Units and Measurements
IEC	International Electrotechnical Commission IMS International Measurement System
ISO	International Organization for Standardization.
LPRI	Laboratoire Primaire de Métrologie des Rayonnements Ionisants, France
NIST	National Institute of Standards and Technology, USA
NPL	National Physical Laboratory, United Kingdom
NRC	National Research Council, Council, Canada
NRL	National Radiation Laboratory, New Zealand
OIML	Organization International de Metrology Legal
PTB	Physikalisch-Technische Bundesanstalt, Germany